An Implantable Magnetic Drive Mechanism for Non-Invasive Arteriovenous Conduit Blood Flow Control

White, Nicholas A.; Van Der Kroft, Sander L.; Van Der Bogt, Koen E.A.; Vrielink, Timo J.C.Oude; Camenzuli, Christian; Sanchez-Margallo, Juan A.; Van De Stadt, Huybert J.F.; Dankelman, Jenny; Rotmans, Joris I.; Horeman, Tim

DOI
10.1109/TBME.2024.3370263

Publication date
2024

Document Version
Final published version

Published in
IEEE Transactions on Biomedical Engineering

An Implantable Magnetic Drive Mechanism for Non-Invasive Arteriovenous Conduit Blood Flow Control

Nicholas A. White, Sander L. van der Kroft, Koen E.A. van der Bogt, Timo J.C. Oude Vrielink, Christian Camenzuli, Jean Calleja-Agius, Juan A. Sánchez-Margallo, Francisco M. Sánchez-Margallo, Huybert J.F. van de Stadt, Jenny Dankelman, Joris I. Rotmans, and Tim Horeman

***Abstract*—*Objective:* Hemodialysis patients usually receive an arteriovenous fistula (AVF) in the arm as vascular access conduit to allow dialysis 2–3 times a week. This AVF introduces the high flow necessary for dialysis, but over time the ever-present supraphysiological flow is the leading cause of complications. This study aims to develop an implantable device able to non-invasively remove the high flow outside dialysis sessions. *Methods:* The developed prototype features a magnetic ring allowing external coupling and torque transmission to non-invasively control an AVF valve. Mock-up devices were implanted into arm and sheep cadavers to test sizes and locations. The transmission torque, output force, and valve closure are measured for different representative skin thicknesses. *Results:* The prototype was placed successfully into arm and sheep cadavers. In the prototype, a maximum output force of 78.9 ± 4.2 N, 46.7 ± 1.9 N, 25.6 ± 0.7 N, 13.5 ± 0.6 N and 6.3 ± 0.4 N could be achieved non-invasively through skin thicknesses of 1–5 mm respectively. The fistula was fully collapsible in every measurement through skin thickness up to the required 4 mm. *Conclusion:* The prototype satisfies the design requirements. It is fully implantable and allows closure and control of an AVF through non-invasive torque transmission. In vivo studies are pivotal in assessing functionality and understanding systemic effects. *Significance:* A method is introduced to transfer large amounts of energy to a medical implant for actuation of a mechanical valve trough a closed surface. This system allows non-invasive control of an AVF to reduce complications related to the permanent high flow in conventional AVFs.**

***Index Terms*—Arteriovenous fistula, Design, Hemodialysis, Implantable device, Transcutaneous energy transmission.**

Manuscript received 8 September 2023; revised 20 November 2023 and 12 February 2024; accepted 14 February 2024. Date of publication 27 February 2024; date of current version 19 July 2024. The work of Joris I. Rotmans was supported in part by NWO (Dutch Research Council) under Take-Off 1 Grant 19810, in part by the Department of BioMechanical Engineering of the Delft University of Technology, in part by the Department of Internal Medicine of the Leiden University Medical Center, and in part by the Delft Health Initiative. *(Tim Horeman and Joris I. Rotmans contributed equally to this work.) (Corresponding author: Tim Horeman.)*

Nicholas A. White and Sander L. van der Kroft are with the Department of BioMechanical Engineering, Delft University of Technology, The Netherlands, and also with the Department of Internal Medicine, Leiden University Medical Centre, The Netherlands.

Koen E.A. van der Bogt is with the Department of Surgery, Leiden University Medical Centre, The Netherlands, also with Haaglanden Medical Centre, The Netherlands, and also with University Vascular Centre Leiden, The Hague, The Netherlands.

Timo J.C. Oude Vrielink and Huybert J.F. van de Stadt are with the Department of Medical Technology, Design and Prototyping, Leiden University Medical Centre, The Netherlands.

Christian Camenzuli is with the Department of Surgery, Faculty of Medicine and Surgery, University of Malta, Malta.

Jean Calleja-Agius is with the Department of Anatomy, Faculty of Medicine and Surgery, University of Malta, Malta.

Juan A. Sánchez-Margallo and Francisco M. Sánchez-Margallo are with Jesús Usón Minimally Invasive Surgery Centre, Spain.

Jenny Dankelman is with the Department of BioMechanical Engineering, Delft University of Technology, The Netherlands.

Joris I. Rotmans is with the Department of Internal Medicine, Leiden University Medical Centre, The Netherlands.

Tim Horeman is with the Department of BioMechanical Engineering, Delft University of Technology, 2628CN Delft, The Netherlands (e-mail: t.horeman@tudelft.nl).

This article has supplementary downloadable material available at https://doi.org/10.1109/TBME.2024.3370263, provided by the authors.

Digital Object Identifier 10.1109/TBME.2024.3370263

I. Introduction

MOST patients suffering from end-stage kidney disease turn to hemodialysis as renal-replacement therapy [1], [2], [3], [4]. For hemodialysis, blood is taken from the body, passed through an external dialysis machine that filters the blood of waste products, after which the 'clean' blood is returned to the body. It is estimated that around 3 million patients are undergoing hemodialysis globally [5].

For chronic hemodialysis, a high-flow and easily accessible vascular access site is necessary, as dialysis is usually performed in 3 sessions of 4 hours per week [6]. In most cases, the arm (Fig. 1) is chosen as the most suitable vascular access site due to the superficiality of the vessels that facilitates frequent cannulation. However, flow through these vessels is to be increased from roughly 30 mL/min to the $>$ 600 mL/min required for hemodialysis [7]. Since 1966 [8], this has been achieved by surgically placing an anastomosis between a major artery and vein in the arm, an arteriovenous fistula (AVF), as shown in Fig. 1(a). The difference in pressure between the artery and vein creates a low resistance pathway for blood that promotes an increased flow through these vessels. After placement, the vein expands over time to accommodate the increased flow through

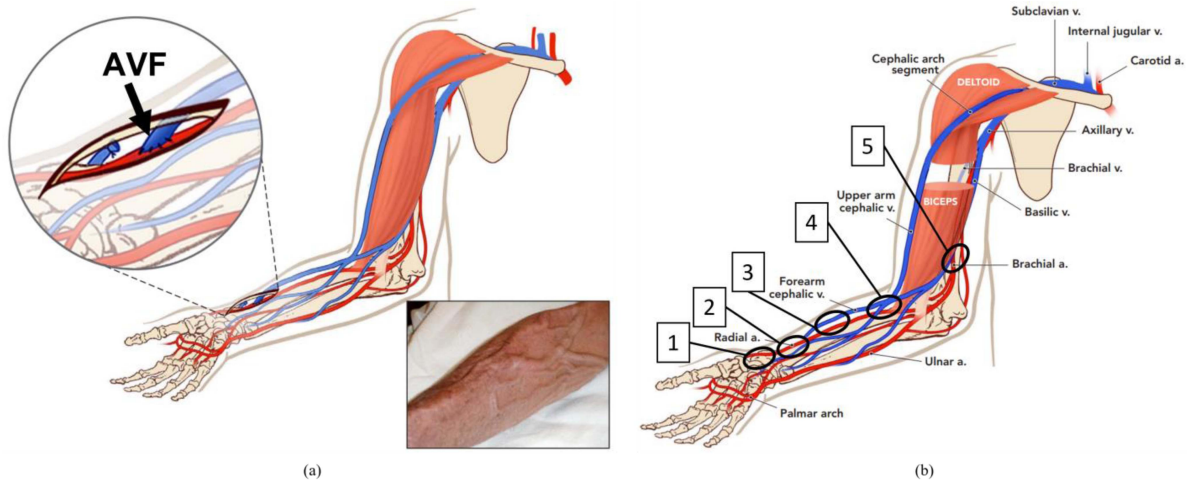

Fig. 1. Graphic representation of (a) an end-to-side arteriovenous fistula (AVF); and (b) locations of AVF placement in the human arm. 1) In the snuffbox. 2) In the wrist. 3) In the forearm. 4) In the elbow fossa. 5) In the medial upper arm. Adapted from [11].

a series of complex mechanisms [9] before usage is possible, known as maturation. If the vein accommodates a flow of $>$ 600 mL/min and has a minimum diameter of 5 mm, the vascular access is considered patent [10]. AVFs can only be placed where major veins and arteries are in close proximity (Fig. 1(b)). The preferred primary placement location is usually the wrist. When the vascular access fails here, more proximal locations can be used, where patency rate is higher, but vascular access-related complications are more frequent [7].

Unfortunately, primary patency of AVFs (i.e., mature and functional without intervention) at 1 year is estimated at only 60% [12], resulting in high reintervention rates due to the necessity of a vascular for hemodialysis, as well as high costs [13]. Moreover, there is a multitude of complications that can hinder functionality or is associated with the presence of the vascular access such as thrombosis, distal ischemia and aneurysms, most of which are linked to the constantly elevated and turbulent flow of blood through the anastomosis [14], [15]. Additionally, a well-functioning vascular access results in a higher burden for the heart, primarily due to the constantly elevated cardiac output, resulting in ventricular hypertrophy [16], [17].

A lot of research has been conducted on improving vascular access outcomes, but no large breakthroughs have taken place since the introduction of the AVF. Most recent innovations focus on optimizing local hemodynamics, but show limited benefits [18], [19]. The supraphysiological flow causing complications remains ever-present, whereas dialysis is only performed for a limited number of hours per week [6]. A vascular access in which the anastomosis can intermittently be opened and closed as shown in Fig. 2, could remove the unfavorable high flow when not in use, while maintaining the functionality of the high-flow vascular access for dialysis. This could greatly improve patient outcomes.

A. Working Principle of the Controllable AVF

Removing the high and turbulent anastomotic flow for the majority of the time is expected to result in a drastically reduced complication rate. However, it must remain possible to increase the flow sufficiently to allow successful dialysis. Simultaneously preventing infection and rejection risks, and additional damage to the anastomosis, e.g., in the form of traction on the sutures and vessels is crucial. Directly compressing the blood vessels is therefore not considered a feasible solution. A very short piece of synthetic graft, used for vascular access in certain cases, will form the anastomosis in a side-to-side fashion, shown in Fig. 2, where fully compressing this graft will block flow and allow circulation to return to normal, while preventing the formation of thrombi (Fig. 3) [20]. Alternatively, the anastomosis could remain in a minimal flow setting as to minimize risks resulting from high flow. Moreover, switching between a fully closed and fully open position and vice versa instantaneously may cause issues relating to changes in blood pressure, so a delay is required. Allowing different stages between fully open and fully closed positions can allow more accurate control and prevent flow greatly exceeding the necessary 600 mL/min.

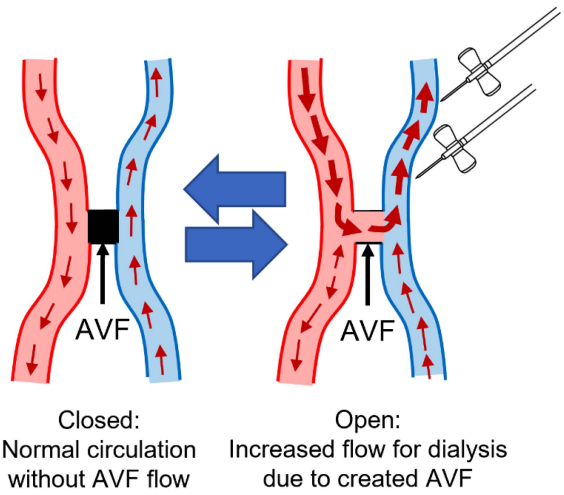

Fig. 2. Illustration of how an adjustable Arteriovenous Fistula (AVF) could control the flow of blood for hemodialysis.

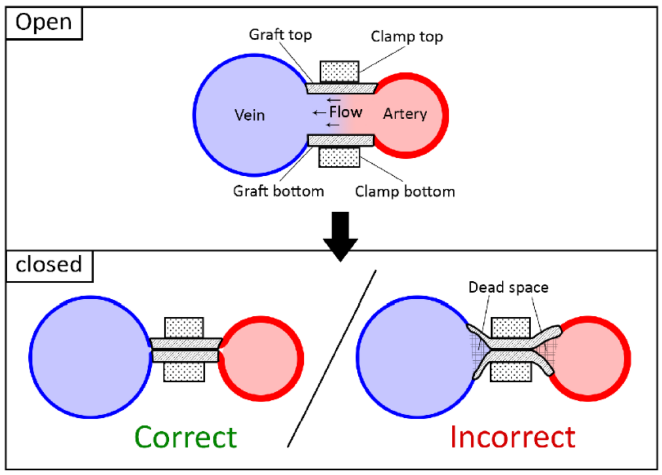

Fig. 3. Illustration of how the AVF should be closed to minimize the risk of thrombus formation in the lumen of the graft outside of dialysis sessions.

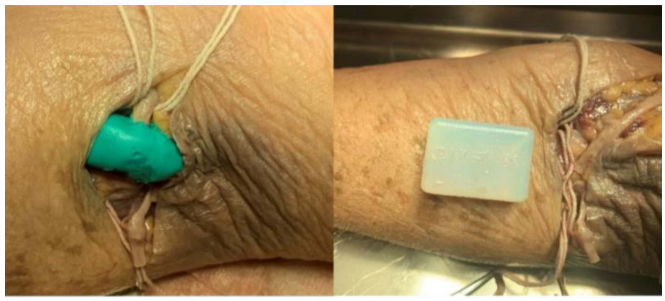

Fig. 4. Incision made in the cubital fossa of a cadaveric arm. The cephalic vein and radial artery are exposed. (a) shows the use of blocks of clay, and (b) shows 3D-printed implant mock-ups utilized to determine the available design space and actuation method of the device to be developed.

The anastomosis is a crucial and fragile anatomical region. Directly applying mechanical force and energy to an implanted actuation device on this area is therefore considered an additional risk. As the outflow vein must remain accessible for frequent cannulation, the decision is made to disconnect the valve mechanism that manipulates the graft from the actuation mechanism, which can be placed at another location along the arm. An added benefit is that the actuation device location is not limited to potential AVF sites and can be placed at locations where more space is available, e.g., in anatomical fossae. The two components can be connected through a flexible transmission cable. Whereas primary vascular access placement is preferred in the wrist, target AVF locations are the elbow fossa in the posterior forearm, and the medial upper arm fossa between the biceps and triceps muscles. These locations are thought to provide more space for an implant, whereas the increased risks of an upper arm AVF relative to the wrist should mostly be mitigated with this concept.

Healthy systolic blood pressure values are already around 120 mmHg (16 kPa), but end-stage kidney disease patients often have the added burden of hypertension [21]. Manipulating the anastomosis to control blood flow will thus require significant mechanical energy. Non-invasive methods of supplying energy to implantable medical devices are currently limited and output is generally low [22], [23], [24], whereas batteries require additional complexity for conversion to mechanical work. Conventional implanted energy supplies will likely make long-term usage of a dynamic AVF infeasible.

B. Contributions

This study provides a design synthesis of a fully implantable device that enables non-invasive transmission of mechanical energy to a valve that is able to control blood flow through an AVF. A unique aspect of this device is the energy transmission mechanism that enables repeated AVF closure over prolonged time. The resulting prototype is ready to be utilized in a large animal model in vivo study to provide insight into biological responses of actuation of mechanical components transcutaneously, as well as intermittently opening and closing an AVF [25]. First an overview of the design requirements is defined, after which the design synthesis and assessment methods of requirements are described, including benchtop experiments and in situ cadaver studies. Finally, results and future perspectives are discussed.

C. Design Requirements

The primary design requirements are as follows:

1. The device must be fully implantable subcutaneously to minimize risks of e.g., infection [26];
2. Energy transmission for actuation of the device is non-invasive, through a skin thickness up to 4.0 mm (SF2) [27];
3. The device manipulates the luminal area of a commercially available graft placed as a side-to-side anastomosis;
4. Anastomotic flow is in the range of 600–1000 mL/min for dialysis when the graft is opened [10];
5. Anastomotic flow is 0 mL/min when the graft is closed, at a pressure of 180 mmHg [28];
6. Resultant forces on the graft and vessels do not cause tearing of anastomotic sutures;
7. There is at least 1 intermediate stage between fully open and fully closed to control flow to a preferential value [7];
8. It takes at least 15 seconds to change the graft from fully open to fully closed [29];
9. Mechanical and biological lifetime of at least 10 years, or 1560 cycles
10. All materials in the device that are in direct contact with bodily fluids and tissues are used in other marketed implants and surgical instruments [30];
11. The device can be cleaned and sterilized according to ISO standards [31];

Additionally, a systematic placement, dimension and skin actuation study was conducted on a cadaveric arm, partially shown in Fig. 4. Supplemental File 1 elaborates this study. The valve dimensions were determined with blocks of clay molded

Fig. 5. 3D-model overview of the actuator component of the prototype and the working mechanism. 1) PEEK hood, 2) neodymium magnets, 3) 3D-printed magnet holder, 4) 316L Stainless Steel (SS) spiral, 5) 316L SS pin and follower, 6) 316L SS backplate and groove for the follower, and 7) external magnets used to apply torque T_e to the actuator through an identical set of magnets. Upon rotating the external magnets, the actuator magnets rotate and guide the pin through the spiral in 1 linear degree of freedom through the groove in the back plate to generate output force $F_p$non-invasively through a gap thickness of$e$. Models were made in SolidWorks (Dassault Systèmes, Paris, France).

to different shapes and dimensions. The actuator dimensions and tactile energy transfer methods were assessed by implanting various 3D-printed models, with the maximum dimensions being found as a 35 mm diameter disk with 10 mm thickness. The results indicate that the maximum dimensions of the valve are: width 10 mm, height 15 mm and length 30 mm. All actuation methods that rely on exerting pressure (e.g., by the fingers) on the skin were considered infeasible as a means of energy transfer. They remain very challenging due to the lack of grip, sliding tissue layers and possible fibrosis formation. Therefore a non-tactile energy transmission through the skin is preferred.

II. Design Synthesis and Experimental Methods

A. Implantable Actuator Mechanism Design

The detailed design of the actuator prototype is shown in Fig. 5. It contains a ring of magnets with alternating pole orientation that can rotate around an axis. Permanent neodymium magnets are chosen due to the high field strength (H = 860–995 kA/m, Supermagnete, Webcraft GmbH, Gotmadingen, Germany) while being readily available. Dimensions are selected to maximize the volume of magnets in a ring configuration in the determined design space. An identical external magnet ring can be coupled to the implant through the skin. When coupled, rotation of the external magnets results in the same rotation of the magnetic wheel in the actuator, transmitting energy non-invasively. The magnets are coated in a very thin layer of silicone glue and placed in a 3D-printed (Dental resin, Form 2, Formlabs, Somerville, MA, USA) wheel, fastened to a CNC-milled 316L Stainless Steel (SS) plate with a spiral groove on the bottom. A SS follower is inserted into this spiral, and is limited to 1 linear degree of freedom by a groove in the SS bottom plate. Through the spiral, rotating the wheel will result in linear displacement of the follower. The dimensional parameters of the actuator and detailed drawings can be found in Supplemental File 2.

As velocities and accelerations should be small, output force can be determined through static equilibrium as shown in Fig. 6(a) and (b):

$$\sum F_x = 0 : F_w = F_N \sin\theta + \mu_s F_N \cos\theta \tag{1}$$

$$\sum F_y = 0 : F_N \cos\theta = F_p + \mu_s F_N \sin\theta. \tag{2}$$

The pitch angle of the spiral thread θ is calculated as:

$$\theta = \tan^{-1}\left(\frac{\delta r}{\delta x}\right) = \tan^{-1}\left(\frac{p}{2\pi r(n)}\right), \tag{3}$$

where p the pitch of the spiral, and $r(n)$ radius of spiral at a specific point in the spiral, calculated as a function of p, the number of revolutions n and the maximum spiral radius$r_{\max}$:

$$r(n) = r_{\max} - p \cdot n \tag{4}$$

Solving for F_p yields:

$$F_p = \frac{F_w(\cos\theta - \mu_s \sin\theta)}{\sin\theta + \mu_s \cos\theta}. \tag{5}$$

Ignoring frictional losses, the transmission of input torque $T_e$to actuator output force F_p can be estimated as

$$F_p = \frac{T_e}{r}\frac{\cos\theta - \mu_s \sin\theta}{\sin\theta + \mu_s \cos\theta}. \tag{6}$$

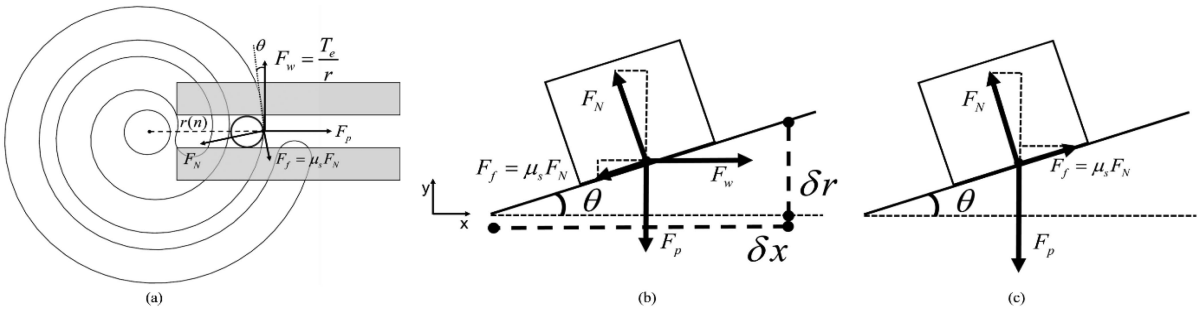

Fig. 6. Free body diagram (FBD) of the pin that moves through the spiral when the spiral is rotated with input torque T_e. The pin is constrained in 1 linear degree of freedom. (a) The pin in the spiral (b) The FBD of the pin when input torque is applied. (c) The FBD of the pin when no input torque is applied.

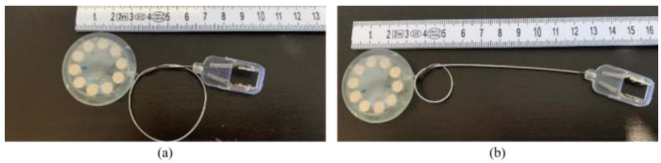

Fig. 7. 3D-printed mock-up of the device with the intended dimensions. If proven necessary, the distance between the valve and actuator component could be made variable by placing a loop with a knot in the transmission cable. (a) Large loop with small distance between components. (b) small loop with larger distance between components. This model was used in cadaver studies to verify fit and placement.

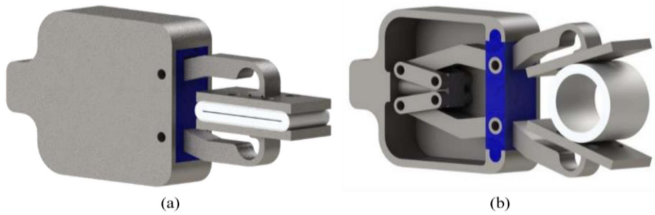

Fig. 8. 3D-model of the valve mechanism with the graft placed between the compressors. (a) The full valve design with side plates, and fully closed graft. (b) The valve without one of the side plates to expose the internal linkage, where the graft is in the fully open position with a relatively low transmission ratio in the linkage. The design of the linkage creates a favorably high transmission ratio that increases when the graft is almost closed. Models were made in SolidWorks (Dassault Systtèmes, Paris, France).

Following Fig. 6(c), when input torque is not applied, static equilibrium is determined by:

$$\sum F_x = 0 : F_N \sin\theta = \mu_s F_N \tag{7}$$

The spiral mechanism is thus stable and non-backdrivable, preventing opening of the valve due to blood pressure or external traction, when $\mu_s \geq \sin\theta$ is satisfied. This equates to $\theta \leq 14°$or a spiral radius of 1.4 mm in the presented configuration with an estimated friction coefficient of 0.25 [32].

A 1 mm thick lathed PEEK cover (a known biocompatible material [33]) with rounded edges and suturing holes is press-fitted over the top of the magnets. A 0.5 mm thick spacer is placed around the central rotation point of this cover to prevent contact friction between the magnets and the cover. Silicone glue is applied to seal the case.

B. Transmission Cable

The transmission cable is a 1 mm diameter flexible spiral grooved 316L SS Bowden cable, with a 0.5 mm 304 SS wire as core. The outer cable is welded to a small cylinder, in turn welded to the base plate of the actuator. The wire core is welded to the pin and follow of the actuator. A small threaded 316L SS cylinder is welded to the other end of the Bowden cable, and another, smaller threaded 316L SS cylinder welded to the wire core. The flexibility of the transmission cable allows a loop to be placed in the cable which enables a change in distance between the valve and actuator components and may decrease resultant forces on the graft and blood vessels, shown in Fig. 7. However, this will result in a significant loss of mechanical efficiency [34] and is not expected to be necessary when placed along the humerus in the upper arm or radius and ulna in the forearm in a human where the anatomy limits relative motion of surrounding tissues.

C. Valve Design

Fig. 8 displays the design of the valve mechanism that is screwed onto the threaded end of the Bowden cable. The outer cable is screwed onto the frame of the valve, and the wire core into a cylinder that is guided linearly through the frame. This is a G6 fitting in which the tolerances are smaller than the diameter of a red blood cell [35], thus should prevent tissue formation inside the casing as no supply of blood is possible. The cylinder is fastened to a linkage functioning as mechanical pinch valve. It supplies force symmetrically to minimize graft displacement, and thus traction on sutures and vessels. Due to the geometry of the graft, the highest compression force is required close to the fully collapsed state. The linkage has a favorable transmission ratio that can achieve this, whereas displacement of external components has been minimized to prevent excessive interaction with adjacent tissues. The exterior parts of the links feature compliant joints which are thought to be more resistant to effects of fibrosis than pinhole joints, but still enable parallel compression and uniform force distribution over the closed graft. Side plates are welded to the frame function both to fasten the

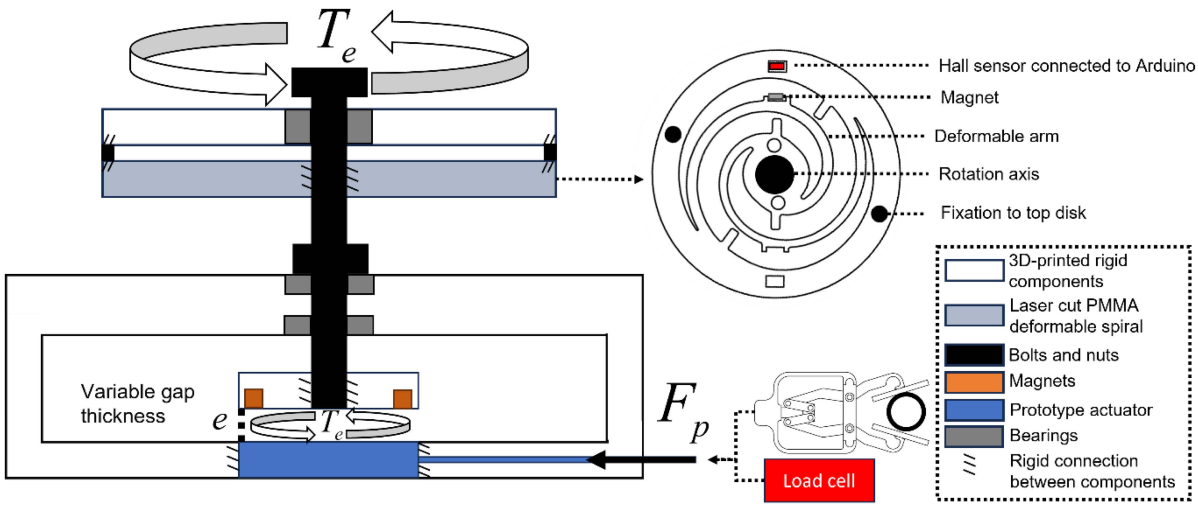

Fig. 9. Schematic cross-sectional overview of the benchtop test setup to measure input torque T_e and output force F_p in the prototype device through different gap thicknesses e. Torque is measured through a spiral with deformable arms, a magnet and Hall sensor, and force is measured through a load cell.

axes around which the links pivot and to create a housing for the linkage. A silicone block is placed between the 2 main pivot points to maintain rotatability while preventing fluid from seeping into the linkage. The compliant joints allow the compressor plates to self-balance into a parallel position to prevent dead space forming when fully closing the graft. A 6 mm internal diameter Acuseal vascular graft (GORE Medical, Flagstaff, AZ, USA) was chosen as prosthetic graft, with the same width as the compressor plates. The graft comprises an elastomer layer between 2 sheets of expanded polytetrafluorethylene (ePTFE). The elastomer layer allows creation of a seal similar to the usage of rubber O-rings. The graft is sutured to the two compressor plates that are welded to the linkage. All components of the valve are titanium and produced with wire electrical discharge machining, except for the cylinder that was processed in a lathe.

D. Development of Test Setup for Benchtop Mechanical Characterization

The device is mechanically characterized in a benchtop force measurement setup. A schematic overview is shown in Fig. 9. The setup contains fixation for the prototype, and a mount for the magnetic coupling, identical to the magnetic ring in the actuator, of which the distance to the prototype can be varied. Silicone sheets of thickness 1.0 mm can be stacked and placed between the magnetic pairs to mimic different thicknesses of skin [36]. The rotation axis of the magnetic coupling is fixed to the mount through a set of ball bearings to minimize friction and restrain motion to 1 rotational degree of freedom.

The input torque supplied to the prototype device is measured through a laser cut polymethyl methacrylate (PMMA) spiral with deformable arms as described in [37] and shown in Fig. 9: a magnet is glued to one of the arms so that the deformation of the spiral from applied torque results in a change in magnetic field on a fixed Hall sensor (OH49E, Ouzhuo, Nanking, China). The sensor is calibrated by applying torque to the exterior of the disk, with the rotational axis connected to a force transducer (QSH02003, FUTEK, Irvine, CA, USA) through a known moment arm. The signal is amplified by a CPJ Strain Gauge Conditioner (Scaime, Juvigny, France) and read in LabVIEW through a NI MyDAQ (National Instruments, Austin, TX, USA). The Hall sensor value is measured through an Arduino NANO (Arduino, Monza, Italy) and read in Arduino software. All data is processed in MATLAB (MathWorks, Natick, MA, USA). A second order polynomial is fit to the calibration data due to the higher order dependency of magnets, Hall sensor distance and Hall sensor values ($R > 0.99$). The calibration data with curve fit and the sensor characteristics can be found in Supplemental File 3.

E. Experimental Validation

1) Dimensions and Implantation: A 3D-printed (Dental Resin, Form 2, Formlabs, Somerville, MA, USA) mock-up of the device with the intended dimensions (Fig. 7) is placed into a single cadaveric human arm (embalmed in formaldehyde) to verify the implantation method and dimensions of the device ex vivo. The authors state that every effort was made to follow all local and international ethical guidelines and laws that pertain to the use of human cadaveric donors in anatomical research. The mock-up includes a 10 cm long transmission cable with a loop to represent the largest dimensions that may be expected. The mock-up of the valve is first sutured to the graft with a suture through each of the suturing holes on the compressor components. An incision is made on the distal and medial side of the cadaver arm. The brachial artery and basilic vein are mobilized to allow placement of a 1 cm piece of vascular graft to be anastomosed. Small incisions are made in both the vein and artery, and the graft is anastomosed between the vessels. Other than the length of graft, this process is identical to standard placement of arteriovenous grafts [7]. A subdermal pocket is created proximally to the anastomosis, and the actuator is sutured

to the cutis through the suturing holes in the PEEK hood. The cable loop is placed parallel to the skin. The wound is then sutured closed. This same mock-up is placed in the neck of a thawed fresh frozen sheep cadaver, where the anastomosis is placed between the carotid artery and external jugular vein, to assess translation of the current prototype to a large animal model for future in vivo assessment.

2) Maximum Torque Transmission: To determine the maximum torque transmission that can be supplied to the implant, the setup shown in Fig. 9 is used. The actuator is exchanged with a magnetic ring identical to that of the setup, covered with a 1.5 mm layer of plastic to compensate for the actuator cover. This ring can rotate freely and is fixed to a load cell through a known moment arm. With 1–5 layers of 1 mm thick silicone to mimic skin, the upper magnetic disk is rotated manually until magnetic decoupling (i.e., slipping) from the lower magnetic disk occurs 20 times. The lower magnetic disk is fastened to a load cell (QSH02003, FUTEK, Irvine, CA, USA) with a known moment arm to determine to the torque supplied, and the signal is amplified (CPJ Strain Gauge Conditioner, Scaime, Juvigny, France) and read. The peak data is retrieved and processed in MATLAB.

3) Maximum Force: The device prototype is placed in the test setup with the valve component detached from the transmission cable. A prototype without cable loop is utilized and the cable remains fixed in the same position in the following experiments. The distal end of the wire core of the transmission cable is fastened to a load cell (QSH02003, FUTEK, Irvine, CA, USA) to measure the maximum output force until decoupling of the magnets occurs. As the actuator spiral contains 2 full rotations, force is measured in 1 full rotation intervals at 0, 1 and 2 rotations, with 1–5 layers of 1 mm thick sheets. Each measurement is performed 5 times. The sensor signal is amplified (CPJ Strain Gauge Conditioner, Scaime, Juvigny, France) and read in LabVIEW through a NI MyDAQ (National Instruments, Austin, TX, USA). The measurements are evaluated against numerical simulations that integrate the measured maximum torque and (6) in MATLAB.

4) Actuation Torque: With the device prototype fastened in the setup (Fig. 9), input torque to actuate the device is measured 1) without the valve fastened, 2) with the valve with no graft placed, 3) with the valve and unpressurised graft, and 4) with the valve pressure pulses of 180/120 mmHg, generated by intermittently decreasing the volume of a closed vessel system. Pressure is measured with a PU5405 pressure gauge (ifm GmbH, Essen, Germany) in LabVIEW through a NI MyDAQ (National Instruments, Austin, TX, USA).

A minimal distance of <0.5 mm between the external magnets and the silicone was kept at all times to prevent contact friction between these surfaces. Measurements are performed by manually rotating the disk for 2 full rotations in intervals of 1/8 rotation. For each instance, the measurement is performed 5 times from open to closed for skin 1–5 mm in 1 mm intervals. In measurements 3) and 4), pressure in the graft is increased to >360 mmHg upon closure. A laser triangulation sensor (optoNCDT 1120, Micro-Epsilon GmbH, Ortenburg, Germany) measures displacement of the distal end of the valve compressor to determine displacement of the valve and verify no leakage occurs resulting from pressure and pulses. A photo is included in Supplemental File 3. The sensor values are processed in MATLAB and torque is estimated by means of the fitted calibration data.

III. Results

The fabricated prototype is shown in Fig. 10.

A. Ex Vivo Cadaver Studies

Shown in Fig. 11, placement of the device at the target locations was possible in both cadavers and tension in the skin resulting from the implants appeared negligible. The actuator unit could easily be identified and external magnetic coupling was possible. Coupling and rotation, and movement of the arm and neck caused no apparent damage to the anastomotic sutures.

B. Maximum Torque Transmission

Fig. 12 displays the measured maximum torque transmission between 2 sets of magnetic rings. The mean $\pm$ standard deviation (SD) that could be transmitted between the Maximum torque transmission sets of magnets were: 0.18 ± 0.009 Nm at 1 mm thickness silicone; 0.10 ± 0.006 Nm at 2 mm; 0.057 ± 0.002 Nm at 3 mm; 0.038 ± 0.002 Nm at 4 mm; and 0.021 ± 0.001 Nm at 5 mm.

C. Maximum Force

Fig. 13 shows the maximum forces estimated and mean $\pm$ SD measured force values at different skin thicknesses and positions in the spiral.

D. Actuation Torque

Fig. 14 displays the measured input torque supplied to the device in the 4 configurations with skin thicknesses 1–5 mm. Up to a skin thickness of 4 mm, the graft could be fully collapsed to block fluid with pressure pulses of 180 mmHg (Fig. 15), but this was not possible with a skin thickness of 5 mm. When the external magnets were replaced by a larger set ($d = 6$ mm, $h = 6$ mm), full graft collapse could be achieved. Fig. 16 shows the relative displacement of the distal end of the valve compressor in closed position when pressure pulses are applied. Displacement remains below 0.01 mm with pressure exceeding 360 mmHg.

IV. Discussion

A prototype has been developed and produced to satisfy the design requirements. This list of requirements was amended following a cadaver study that provided preliminary information on maximum dimensions and energy transmission methods. The presented device is fully implantable and allows non-invasive closure and control of a synthetic graft. The device is non-backdrivable and the graft can remain stable in every position between fully open and fully closed. Motion of the device and its components have been minimized to prevent effects of fibrosis tissue formation, pain and interaction with fragile tissues such as nerves. From an anatomical point of view, there are no adjacent nerves in the antecubital fossa in the forearm (the

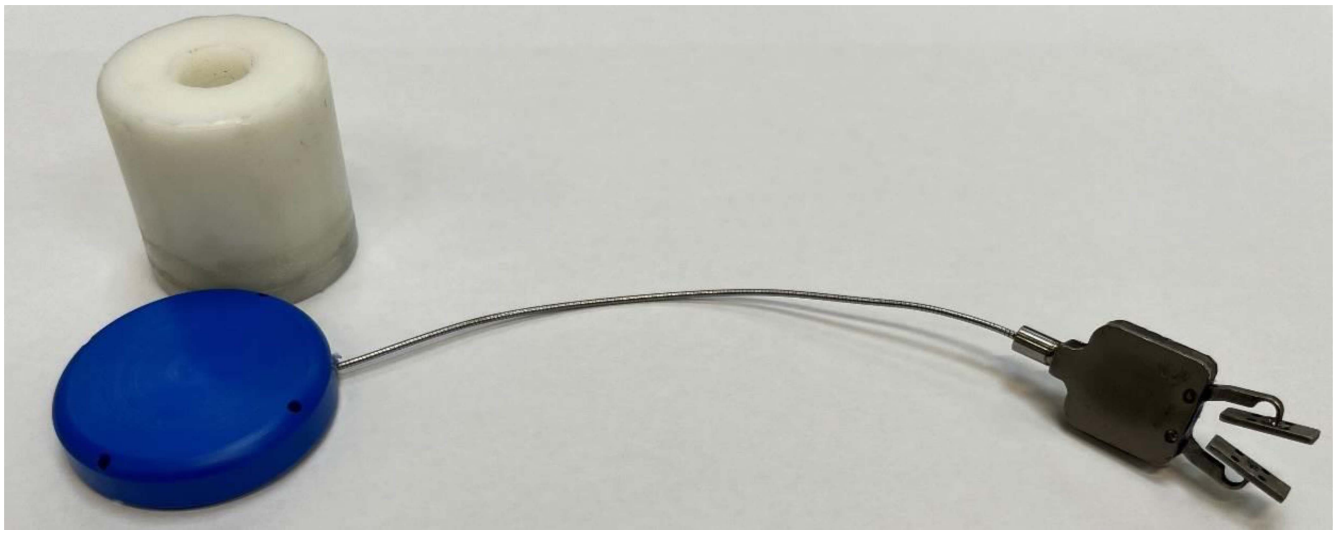

Fig. 10. Manufactured prototype of the implant device used in the experimental setup, and the external magnets that can be utilized to actuate the prototype.

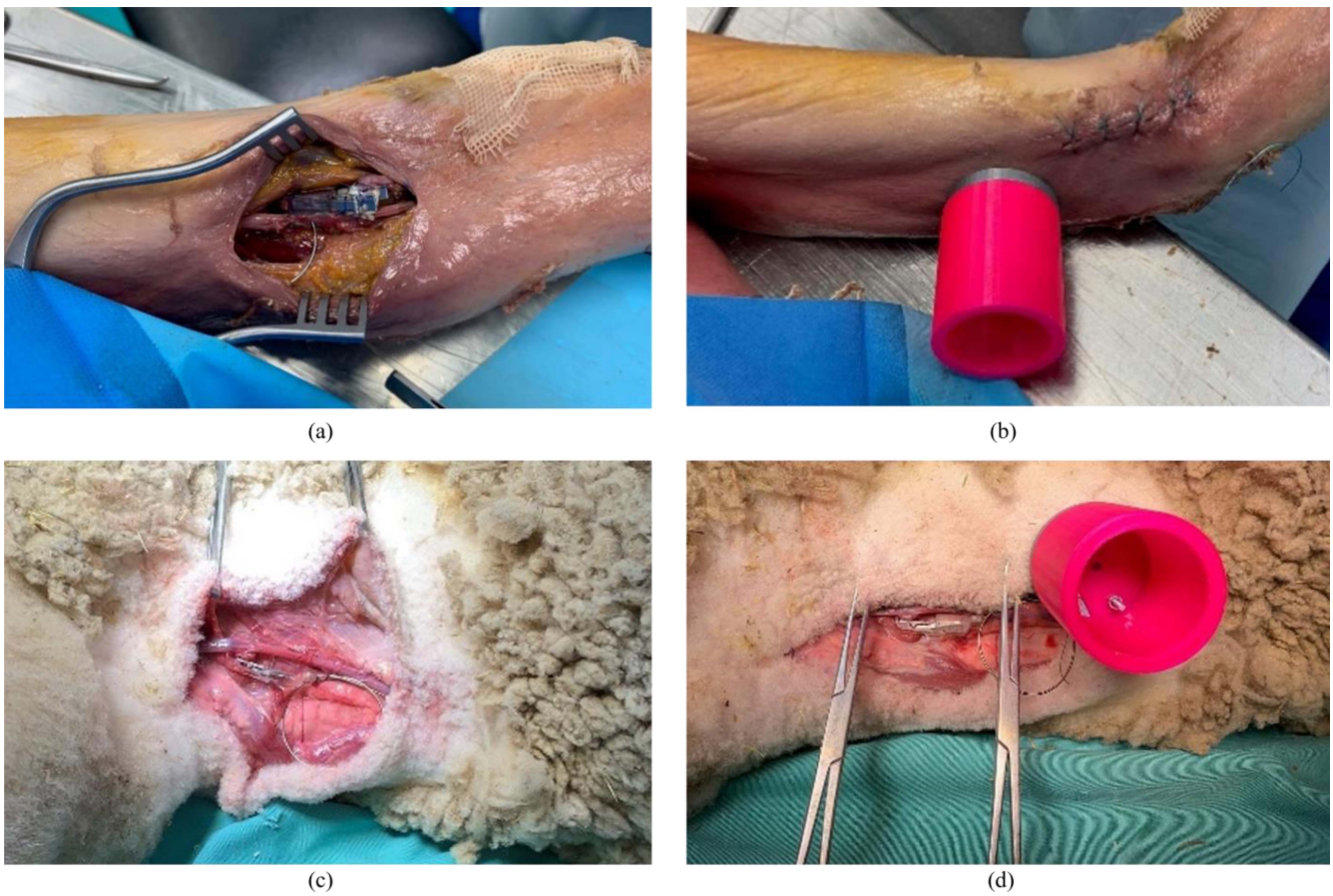

Fig. 11. Cadaver arm (top) and sheep (bottom) with the mock-up of the device implanted. (a) The surgical incision created on the medial side of the upper arm between the biceps and triceps, with the valve anastomosed between the brachial artery and basilic vein in the distal upper arm and the actuator in a subdermal pocket proximal to the shoulder. (b) The closed incision and magnets easily coupled through the skin. (c) The surgical incision on the anterolateral side of the neck of the sheep, with the valve anastomosed between the carotid artery and external jugular vein cranially and the actuator in a subdermal pocket proximal to the chest. (d) The skin be placed over the implant, showing coupling with the external magnets is still possible.

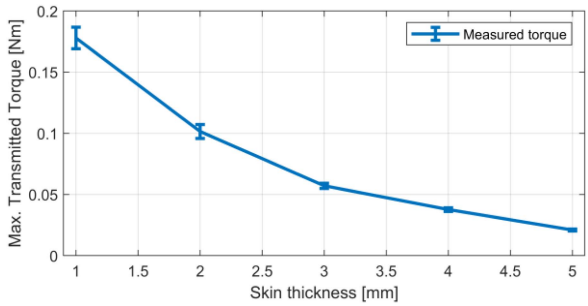

Fig. 12. Average ± standard deviation of the maximum torque transmitted between the sets of magnetic rings through 1–5 mm thickness of silicone skin model.

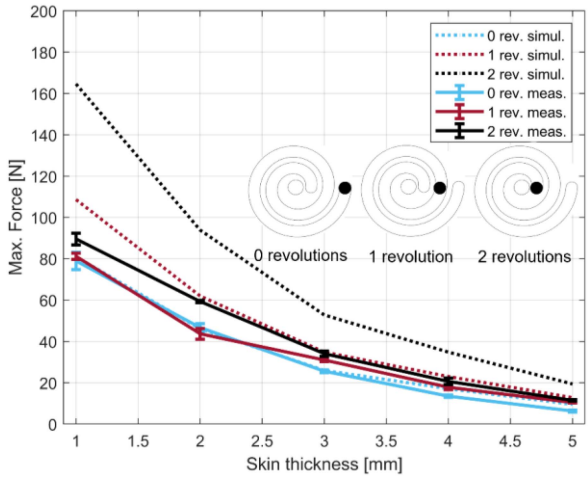

Fig. 13. Simulated and measured average ± standard deviation of the maximum force generated on the transmission cable by the actuator components at various position in the spiral and through 1–5 mm thickness of silicone skin model.

target implantation site). In the upper arm, the device can be safely implanted between the brachial artery and the basilic or cephalic vein without interference with the median nerve, which typically presents more dorsally. After placement, migration of the components as well as the encapsulation of the materials should be monitored over time.

Due the large number of uncertainties and unknowns remaining, the focus of the prototype is to provide more data and supplement the requirements list in upcoming in vivo studies [25], for example relating to fibrous tissue formation and biological responses to the energy transmission and manipulating the AVF. Currently, the device dimensions and choice of transmission are based on a study of a single cadaveric arm. As almost all dimensions tested could be implanted, the maximum dimensions may be larger than tested in this study. Although subjective, this study suggested tactile energy transmission was not feasible. However, the effect of the embalming cannot be neglected as this could have reduced the frictional coefficient of the skin. Moreover, fibrous tissue forms around foreign material upon implanting, which will more rigidly encapsulate the implant in the surroundings and may affect the feasibility of external tactile manipulation. The dimensional requirements and placement method were verified by implanting a mock-up of the device into a second cadaveric arm, but anatomical variations have not been taken into account. Even though the force and pressure applied to the skin are considerably lower than the generated force, it is crucial to acknowledge that pain and pressure ulcers (decubitus) are risks of the transmission method. It is worth mentioning that the force application duration is much shorter than typically known to cause decubitus [38]. The actuator is fixed with sutures and edges are rounded as preventative measures. A thin, low friction skin pad may also be added to reduce shear forces and stresses on the skin during actuation. These phenomena may be further assessed in future studies. The mechanical tests included silicone rubber sheets to mimic skin as the magnetic properties are similar [36]. The exponential curve of the measured torque values seen in Fig. 12 may be considered representative of the higher-order dependence of magnetic attraction versus distance. This data was used to estimate the maximum force that could be supplied by the actuator in (1) and (6). These equations predict that the actuator can supply a higher force when the pin and follower approach the center of the spiral where the moment arm is at its smallest. Fig. 13 shows the measurements with a similar pattern as the simulation, but the overestimation in the calculations is larger when the spiral radius is smaller. In part, this may be explained by the presence of friction in the benchtop model. In reality force in the cable is generated through a stick-slip motion between the pin and the spiral: torque is applied to overcome static friction as in Fig. 6(b), and the pin rests in the position in Fig. 6(c) until sufficient torque is applied to overcome friction again. In the experimental setup, each slip pulls the pin further inwards, which results in a slight elongation of the cable and an increase in force on the load cell. Hereafter the pin returns to the static position of Fig. 6(c). When the radius of the spiral is larger, the pitch angle θ is smaller following (1). The pin therefore faces a steeper gradient closer to the rotation axis: for the same tangential displacement to slip and stick, δx, the radial displacement δr is larger. In other words, the radial component of the frictional force F_f increases with decreasing r, meaning greater force is necessary to overcome static friction and advance the pin inwards through the spiral. This phenomenon has not been accounted for in the calculations and results in an overestimation of the actual force that can be realized close to the rotational axis of the spiral. The coefficient of friction between the spiral and the following pin has a large impact on the force transmission and the efficiency. In the current model this has been estimated from literature as a constant value of in 316L SS to 316L SS [32]. However, this is more complex in reality and depends largely on the surface finish, lubrication, and forces [32]. In future models this coefficient may be determined experimentally in this configuration.

Fig. 14(a) and (b) show the torque necessary to overcome the internal resistance of actuator and the actuator with valve when unloaded. Unsurprisingly this resistance is higher with the valve as the valve adds additional resistance due to the moving components. Following Fig. 14(c) and (d), placing the graft adds more resistance, and applying pressure to the graft further increases the necessary actuation torque. The patterns

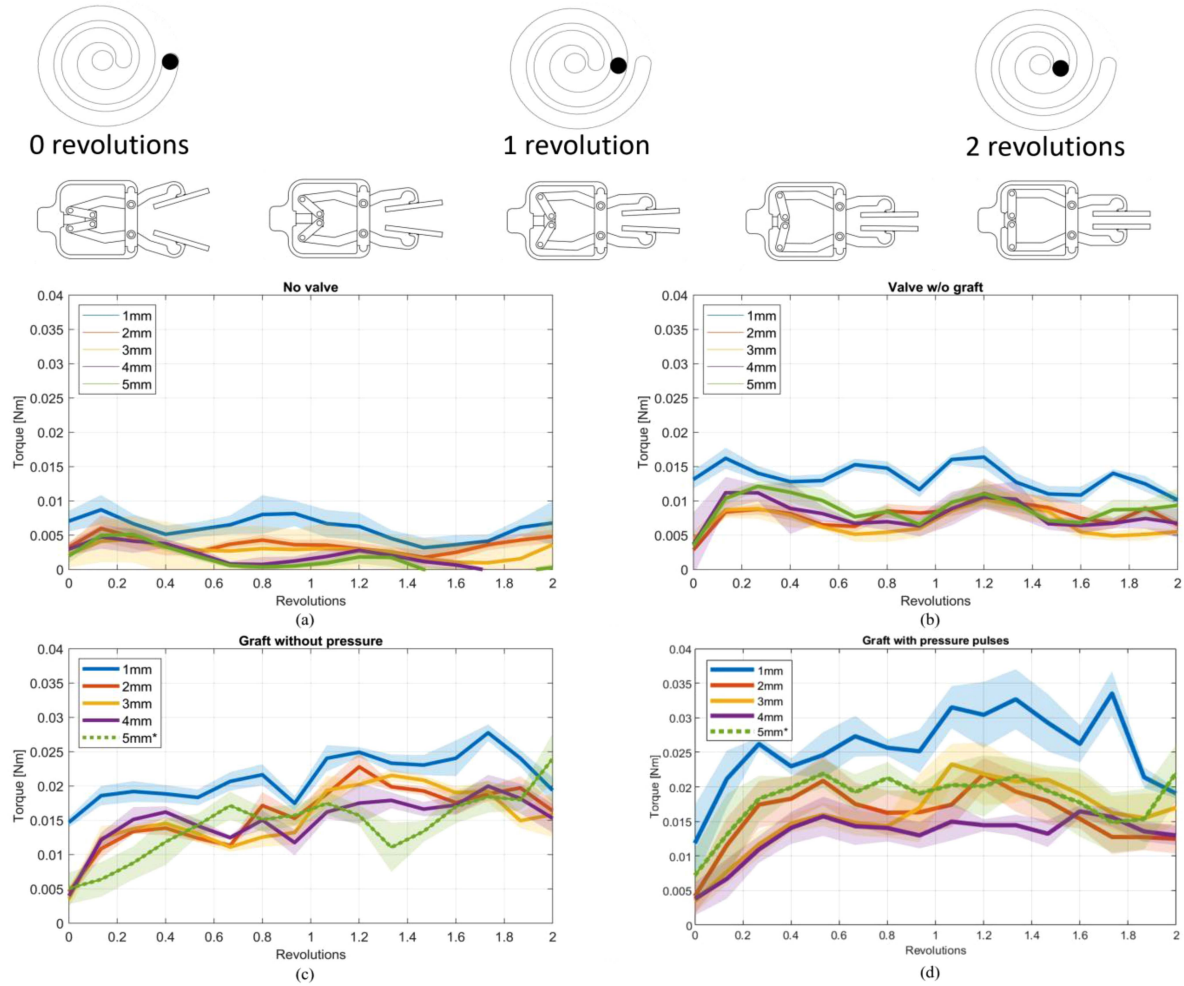

Fig. 14. Torque measurements. Top: the position of the valve at pin positions in the actuator spiral. Bottom: the measured input torque required to fully actuate the device with silicone skin model thickness 1–5 mm in: (a) the actuator without the valve component connected; (b) the actuator with the valve connected; (c) the actuator and valve with an unpressurised graft placed between the compressors; and (d) the actuator and valve with graft pressurized to 180 mmHg. ∗indicates a different external magnet configuration was used than in the other measurements.

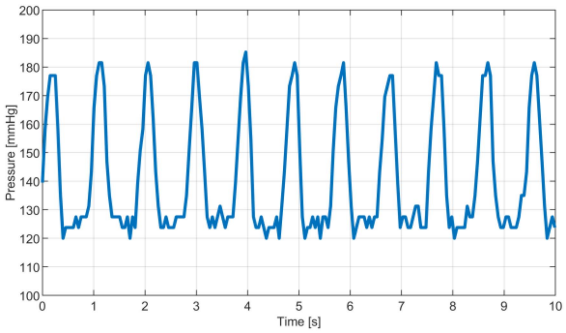

Fig. 15. Measurement of the pressure profile applied to the synthetic graft at 63 beats per minute in the torque measurement of the prototype device in Fig. 14(d).

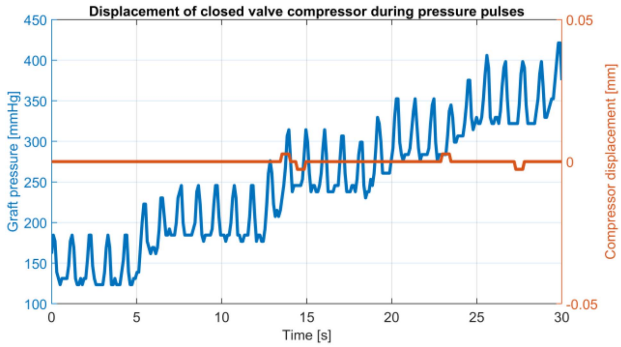

Fig. 16. Measurement of the pressure profile applied to the synthetic graft at 63 beats per minute and the resulting displacement of the distal end of the compressor of the closed valve.

appear similar in all measurements with the graft placed, and can be related to the transmission of forces to the graft by the valve; the torque pattern is an integration of the resistance of the graft, and internal resistance and the transmission ratio of the device. The internal resistance is in part a result of manufacturing imperfections.

The design requirement was to fully collapse a graft at 180 mmHg through a skin thickness of 4 mm, which included

a safety factor of 2. A pulsatile pressure of 180/120 mmHg in a used to simulate in vivo working conditions. A closed system was used in which pressure is equal in all directions throughout the system. The pressure was representative of arterial pulses in the context of the design requirement, where primarily the pressure tangential to the graft surface is of interest. The pressure pulses did not result in leakages through the closed valve. However, the variation in input torque was larger with the pulsatile flow (Fig. 14(d)), which may be explained by the pressure variations. Future evaluation may include fluidic flow at such pressures as an improved representation. However, Fig. 16 shows that there was no displacement of the compressor of the closed valve even with pressure pulses exceeding 360 mmHg, suggesting no leakage is possible well within the requirement and safety factor, and the device is non-backdrivable.

In the test setup it was found that collapse was feasible up to a thickness of 4 mm, and no longer possible with a thicker skin. When utilizing larger magnets to actuate the prototype it was possible to collapse the graft with a skin thickness of 5 mm, demonstrating that some design freedom remains in the external component to further optimize energy transmission. Additionally, the configuration of magnets was chosen to be maximized for the determined design space. In the experiments torque transmission and force generation was found to exceed the requirements. Therefore, future iterations should feature a bottom-up approach to optimize the magnetic transmission. In situ cadaver studies showed that placement of the device was possible in both a human arm and sheep neck. A larger incision and an adjusted surgical protocol for the anastomotic surgery were necessary. This will likely have adverse effects when used in patients and will need to be studied separately to address benefit-risk ratio of the implant. The resultant forces on the anastomosis and sutures were only assessed in the cadaver studies shown in Fig. 11. Even though excessively moving the cadavers did not show any apparent damage to the sutures, this model did not include actuation of the valve component. However, the linkage has been designed in a symmetric configuration to minimize lateral displacement, and therefore traction on the anastomotic sutures. Although the cable forces necessary to actuate the valve and close the graft are significant, the outer sheath of the Bowden cable compensates for these forces [39] to minimize traction on the anastomosis. This should be formally assessed in future studies.

For in vivo applications the device will require assembling in a clean environment. As the actuator contains magnets and tight-fitting components of different materials, gamma or other low temperature sterilization will be feasible methods of sterilization because the high temperatures of other methods could result in demagnetization of fracture of components. Although it has not yet been assessed, it is expected that meeting relevant standards should be possible. However, this requires validation, and the optimal dose to achieve sterilization standards may be found experimentally.

Due to the inclusion of magnets in the actuation device, certain procedures such as magnetic resonance imaging will not be possible. The clinical implications of this drawback are expected to be limited, and outweighed by the potential benefits of removing anastomotic flow, but requires formal assessment.

Lifetime was set as a requirement for the device, but this has not yet been evaluated as it is likely affected greatly by in vivo factors, e.g., toxicity, foreign body response and everyday use. Increasing tissue layer thickness between the implant and external magnets, e.g., due to fibrosis, remains a risk factor for the transmission. To advance development of the device, in vivo studies are imperative to assess biocompatibility and better understand systemic response to intermittently closing an AVF, but also to study functionality of moving mechanical components and magnetic energy transfer.

While the device is eventually to be used in humans, the necessity of animal studies and anatomical and biological differences with the animal model cannot be ignored. The current prototype has been designed to take these into account, for example by allowing skin to be thicker through stronger external magnets, but also with a loop in the transmission cable when a different implant location must be used. These studies may therefore be conducted with minimal changes and safety and mechanical performance data should be translatable to human use. Goats are to be used as AVF models due to similarities in size, thrombogenicity, vascular response and skin thickness, while being even more prone to stenosis formation [40]. If used, placement will occur in the neck as shown in Fig. 11(c) and (d) due to the proximity, diameters and superficiality of vein and artery.

A novel method for non-invasively transferring large amounts of energy to a medical implant and generating a high force has been demonstrated, which is an advantage when compared to existing energy transfer methods that are limited to low energy outputs [21], [22], [23]. While the current study focuses on the use of this method for AVF closure through a mechanical pinch valve, the actuation device could find application in other use cases, or inspire the development of novel implantable devices that require high energy transmission and forces.

V. Conclusion

A fully implantable magnetic actuator-effector device has been presented, which enables non-invasive transfer of energy through the skin and can be used to actuate a mechanical valve system or potentially other types of end-effectors. Through this actuator, a valve component that manipulates an AVF for dialysis can be non-invasively controlled. The focus of the device was to be utilized in large animal model in vivo experiments to assess biological responses to intermittently closing the AVF, magnetic actuation, and moving mechanical components. The maximum dimensions and actuation method for non-invasive energy transfer were determined through a study on a single cadaveric arm. The developed prototype features a ring of magnets that can be controlled by an identical ring of magnets from outside the body. Rotation of these magnets can generate the high force required to fully close a short piece of synthetic graft as AVF. Benchtop and in situ experiments showed that the device meets the design requirements, and should be suitable for use in upcoming in vivo animal studies.

Acknowledgment

The authors would like to express their gratitude to prof. M.C. de Ruiter and A.A.H. Immerseel of the department of Anatomy at the Leiden University Medical Center, and D. Durán-Rey of Jesús Usón Minimally Invasive Surgery Centre for facilitating the animal model cadaver study.

References

[1] R. Saran et al., "US Renal Data System 2016 Annual Data Report: Epidemiology of Kidney disease in the United States," *Amer. J. Kidney Dis.*, vol. 69, no. 3, pp. A7–A8, 2017, doi: 10.1053/j.ajkd.2016.12.004.

[2] R. Pecoits-Filho et al., "Capturing and monitoring global differences in untreated and treated end-stage kidney disease, kidney replacement therapy modality, and outcomes," *Kidney Int. Suppl.*, vol. 10, no. 1, pp. e3–e9, 2020, doi: 10.1016/j.kisu.2019.11.001.

[3] A. K. Bello et al., "Status of care for end stage kidney disease in countries and regions worldwide: International cross sectional survey," *BMJ*, vol. 367, 2019, Art. no. 5873, doi: 10.1136/bmj.l5873.

[4] A. K. Bello et al., "Assessment of global kidney health care status," *J. Amer. Med. Assoc.*, vol. 317, no. 18, pp. 1864–1881, 2017, doi: 10.1001/jama.2017.4046.

[5] A. K. Bello et al., "Epidemiology of haemodialysis outcomes," *Nature Rev. Nephrol.*, vol. 18, no. 6, pp. 378–395, Feb. 2022, doi: 10.1038/s41581-022-00542-7.

[6] J. Tattersall et al., "EBPG guideline on dialysis strategies," *Nephrol. Dialysis Transplant.*, vol. 22, no. SUPPL.2, 2007, pp. ii5–ii21, doi: 10.1093/ndt/gfm022.

[7] C. E. Lok et al., "KDOQI Clinical Practice Guideline for Vascular access: 2019 update," *Amer. J. Kidney Dis.*, vol. 75, no. 4, pp. S1–S164, Apr. 2020, doi: 10.1053/J.AJKD.2019.12.001.

[8] M. J. Brescia et al., "Chronic hemodialys using venipuncture and a surgically created arteriovenous fistula," *New England J. Med.*, vol. 275, no. 20, pp. 1089–1092, 1966, doi: 10.1056/NEJM196611172752002.

[9] Y.-T. Shiu et al., "Arteriovenous conduits for hemodialysis: How to better modulate the pathophysiological vascular response to optimize vascular access durability," *Amer. J. Physiol. Renal Physiol.*, vol. 316, no. 5, pp. F794–F806, May 2019, doi: 10.1152/AJPRENAL.00440.2018.

[10] I. D. Maya and M. Allon, "Vascular Access: Core curriculum 2008," *Amer. J. Kidney Dis.*, vol. 51, no. 4, pp. 702–708, 2008, doi: 10.1053/j.ajkd.2007.10.046.

[11] T. Vachharajani, "Atlas of dialysis vascular access," 2010. Accessed: Aug. 17, 2023. [Online]. Available: http://c.ymcdn.com/sites/www.asdin.org/resource/resmgr/imported/atlas%20of%20dialysis%20access.pdf

[12] A. A. Al-Jaishi et al., "Patency Rates of the arteriovenous fistula for hemodialysis: A systematic review and meta-analysis," *Amer. J. Kidney Dis.*, vol. 63, no. 3, pp. 464–478, Mar. 2014, doi: 10.1053/J.AJKD.2013.08.023.

[13] D. Schon et al., "Increasing the use of arteriovenous fistula in hemodialysis: Economic benefits and economic barriers," *Clin. J. Amer. Soc. Nephrol.*, vol. 2, pp. 268–276, 2007, doi: 10.2215/CJN.01880606.

[14] T. C. Rothuizen et al., "Arteriovenous access failure: More than just intimal hyperplasia?," *Nephrol. Dialysis Transplant.*, vol. 28, no. 5, pp. 1085–1092, May 2013, doi: 10.1093/NDT/GFT068.

[15] R. Stolic, "Most important chronic complications of arteriovenous fistulas for hemodialysis," *Med. Princ. Pract.*, vol. 22, no. 3, pp. 220–228, 2013, doi: 10.1159/000343669.

[16] M. Cozzolino et al., "Cardiovascular disease in dialysis patients," *Nephrol. Dialysis Transplant.*, vol. 33, pp. iii28–iii34, 2018, doi: 10.1093/ndt/gfy174.

[17] B. M. Voorzaat et al., "The pros and cons of preserving a functioning arteriovenous fistula after kidney transplantation," *J. Vasc. Access*, vol. 17, no. 1, pp. S16–S22, 2016, doi: 10.5301/jva.5000525.

[18] R. Shahverdyan, T. Meyer, and V. Matoussevitch, "Patency and functionality of radiocephalic arteriovenous fistulas with an external support device (VasQTM): Real-world single-center experience," *J. Vasc. Access*, vol. 22, no. 2, pp. 166–172, Mar. 2021, doi: 10.1177/1129729820904599.

[19] R. Shahverdyan, P. Tabbi, and G. Mestres, "Multicenter European real-world utilization of VasQ anastomotic external support device for arteriovenous fistulae," *J. Vasc. Surg.*, vol. 75, no. 1, pp. 248–254, 2022, doi: 10.1016/j.jvs.2021.07.120.

[20] B. Furie and B. C. Furie, "Mechanisms of thrombus formation. Mechanisms of disease," *New England J. Med.*, vol. 359, no. 9, pp. 938–949, 2008. [Online]. Available: http://www.ncbi.nlm.nih.gov/pubmed/18753650

[21] A. S. Go et al., "Chronic kidney disease and the risks of death, cardiovascular events, and hospitalization," *New England J. Med.*, vol. 351, no. 13, pp. 1296–1305, 2004, doi: 10.1056/nejmoa041031.

[22] O. V. Gorskii, "Potential power supply methods for implanted devices," *Biomed. Eng.*, vol. 52, no. 3, pp. 204–209, 2018, doi: 10.1007/s10527-018-9814-z.

[23] S. N. Suzuki, M. Ishihara, and Y. Kobayashi, "The improvement of the noninvasive power-supply system using magnetic coupling for medical implants," *IEEE Trans. Magn.*, vol. 47, no. 10, pp. 2811–2814, Oct. 2011, doi: 10.1109/TMAG.2011.2151273.

[24] Y. Lu, Y. Jia, and C. Yu, "Recent advances in power supply strategies for untethered neural implants," *J. Micromechanics Microeng.*, vol. 31, no. 10, 2021, Art. no. 104003, doi: 10.1088/1361-6439/ac1c92.

[25] N. A. White et al., "Question-based development of high-risk medical devices: A proposal for a structured design and review process," *Brit. J. Clin. Pharmacol.*, vol. 89, no. 7, pp. 2144–2159, 2023, doi: 10.1111/bcp.15685.

[26] L. Affeld et al., "Percutaneous devices: A review of applications, problems and possible solutions," *Expert Rev. Med. Devices*, vol. 9, no. 4, pp. 389–399, 2012, doi: 10.1586/erd.12.25.

[27] K. H. Sim et al., "The appropriateness of the length of insulin needles based on determination of skin and subcutaneous fat thickness in the abdomen and upper arm in patients with type 2 diabetes," *Diabetes Metab. J.*, vol. 38, no. 2, pp. 120–133, 2014, doi: 10.4093/DMJ.2014.38.2.120.

[28] American Heart Association, "Understanding blood pressure readings | American Heart Association," 2017, Accessed: Jul. 25, 2023. [Online]. Available: https://www.heart.org/en/health-topics/high-blood-pressure/understanding-blood-pressure-readings

[29] A. C. Guyton and K. Sagawa, "Compensations of cardiac output and other circulatory functions in areflex dogs with large AV fistulas," *Amer. J. Physiol.*, vol. 200, pp. 1157–1163, 1961, doi: 10.1152/ajplegacy.1961.200.6.1157.

[30] European Parliament and Council, "Regulation (EU) 2017/745 on medical devices, amending Directive 2001/83/EC, Regulation (EC) No 178/2002 and Regulation (EC) No 1223/2009 and repealing Council Directives 90/385/EEC and 93/42/EEC," *Official J. Eur. Union*, vol. 117, pp. 1–175, Apr. 2017. [Online]. Available: http://data.europa.eu/eli/reg/2017/745/oj[legislation]

[31] International Organization for Standardization, "implants for surgery - active implantable medical devices - part 1: General," 2014.

[32] M. Fellah et al., "Tribological behaviour of AISI 316L stainless steel for biomedical applications," *Tribol. - Mater. Surfaces Interfaces*, vol. 7, no. 3, pp. 135–149, 2013, doi: 10.1179/1751584X13Y.0000000032.

[33] J. M. Toth, "Biocompatibility of PEEK polymers," in *PEEK Biomaterials Handbook*, 2nd ed. Norwich, NY, USA: William Andrew Publishing, 2019, Chapter. no. 8, pp. 107–119.

[34] P. Letier et al., "Bowden cable actuator for torque-feedback in haptic applications," in *Proc. Eurohaptics*, 2006, pp. 1–6.

[35] M. Diez-Silva et al., "Shape and biomechanics characteristics of human red blood cells in health and disease," *MRS Bull.*, vol. 35, no. 5, pp. 382–388, 2010, doi: 10.1557/mrs2010.571.

[36] A. K. Dabrowska et al., "Materials used to simulate physical properties of human skin," *Skin Res. Technol.*, vol. 22, no. 1, pp. 3–14, 2016, doi: 10.1111/srt.12235.

[37] T. Horeman et al., "Force sensing in surgical sutures," *PLoS One*, vol. 8, no. 12, pp. 1–12, 2013, doi: 10.1371/journal.pone.0084466.

[38] C. Bansal et al., "Decubitus ulcers: A review of the literature," *Int. J. Dermatol.*, vol. 44, no. 10, pp. 805–810, 2005, doi: 10.1111/j.1365-4632.2005.02636.x.

[39] D. Chen, Y. Yun, and A. D. Deshpande, "Experimental characterization of bowden cable friction," in *Proc. IEEE Int. Conf. Robot. Automat.*, 2014, pp. 5927–5933.

[40] W. J. Geelhoed et al., "A novel method for engineering autologous non-thrombogenic in situ tissue-engineered blood vessels for arteriovenous grafting," *Biomaterials*, vol. 229, 2020, Art. no. 119577, doi: 10.1016/j.biomaterials.2019.119577.